Controlled Ion Fragmentation in a 2-D Quadrupole Ion Trap for External Ion Accumulation in ESI FTICR Mass Spectrometry

Mikhail E. Belov, Michael V. Gorshkov,* Harold R. Udseth, and Richard D. Smith

Environmental Molecular Sciences Laboratory, Pacific Northwest National Laboratory, Richland, Washington, USA

Undesired fragmentation of electrospray generated ions in an rf multipole traps can be problematic in many applications. Of special interest here is ion dissociation in a 2-D quadrupole ion trap external to a Fourier transform ion cyclotron resonance mass spectrometer (FTICR MS) used in proteomic studies. In this work, we identified the experimental parameters that determine the efficiency of ion fragmentation. We have found that under the pressure conditions used in this study there is a specific combination of the radial and axial potential well depths that determines the fragmentation threshold. This combination of rf and dc fields appears to be universal for ions of different mass-to-charge ratios, molecular weights, and charge states. Such universality allows the fragmentation efficiency of the trapped ions in the course of capillary liquid chromatography (LC) separation studied to be controlled and can increase the useful duty cycle and dynamic range of a FTICR mass spectrometer equipped with an external rf only 2-D quadrupole ion trap. (J Am Soc Mass Spectrom 2001, 12, 1312–1319) © 2001 American Society for Mass Spectrometry

When combined with high-performance separations (e.g., using liquid chromatography, or capillary isoelectric focusing), Fourier transform ion cyclotron resonance mass spectrometry (FTICR) provides a powerful tool for proteomic studies [1–3]. In one powerful approach proteins are digested with trypsin and the separated tryptic peptides are then introduced on-line to an electrospray ionization (ESI) source of an FTICR mass spectrometer. The sensitivity, dynamic range, and duty cycle provided by FTICR have been shown to be increased by ion trapping and accumulation in a 2-D multipole ion trap positioned externally to an FTICR cell [4–7]. However, ion fragmentation in an rf only multipole (e.g., a hexapole) during extended accumulation periods [8] imposes constrains for the use of external ion accumulation with FTICR. The problem is exacerbated for on-line capillary LC separations coupled to a FTICR with an external accumulation interface. The ion production rate from capillary LC separations of protein digests varies unpredictably by more than two orders of magnitude. This requires longer ion accumulation times to fully utilize the charge capacity of an external ion trap (i.e., to enhance the dynamic range). Higher duty cycles can be accomplished by ion accumulation in the external ion trap for increased ion accumulation periods (~1 s), potentially accompanied by ion fragmentation. Taking into account the peak capacity of high-performance LC separations (~1000 [9, 10]), such fragment ion peaks can result in possible data misinterpretation. Therefore, fragmentation of ions trapped in an rf only multipole for extended periods should be minimized.

Significant progress in understanding ion fragmentation mechanisms has been made using linear quadrupole collision cells in the fly-thru mode [11–14]. Ion fragmentation has been attributed to ion neutral collisions in the axial field gradient at the entrance of a quadrupole collision cell operated at $\sim 10^{-2}$ torr [15] and an optimum pressure was found to increase ion transmission through an rf only quadrupole [16]. It should be noted that the rf field is mostly used in higher-pressure rf only quadrupole collision cells for the radial confinement of a traversing ion beam.

Ion fragmentation in 3-D ion traps has been studied for a number of years [17–21]. Using the approach of boundary effect activated dissociation [21], ions were excited by a short dc pulse to the boundary of the ion

Published online October 18, 2001

Address reprint requests to Dr. R. D. Smith, Environmental Molecular Sciences Laboratory, Pacific Northwest National Laboratory, MS K8-98, P. O. Box 999, Richland, WA 99352, USA. E-mail: rd_smith@pnl.gov

*Visiting scientist from Institute of Energy Problems of Chemical Physics, Russian Academy of Sciences, Moscow 117829, Russia.

1044-0305/01/$20.00
PII S1044-0305(01)00318-X

Received April 19, 2001
Revised August 1, 2001
Accepted August 1, 2001

stability diagram resulting in an increase in the amplitude of oscillations (where the direction of oscillations is determined by the polarity of the dc pulse). The increase in the amplitude of oscillation results in higher energy collisions with the buffer gas and fragmentation of ions within the boundary region. Also, increasing the ion population in a 3-D ion trap (i.e., higher space charge) has been found to distort its ion stability diagram [22–24], thus causing ion fragmentation at low q_z (i.e., lower rf amplitudes).

As ions are accumulated in an rf only multipole for longer times, the increasing space charge drives ion cloud radial expansion. Similar to boundary effect activated dissociation in 3-D ion traps, higher rf field potentials at larger radii cause ions to oscillate to larger amplitudes, thereby pushing them to higher kinetic energies and causing fragmentation due to collisions with the buffer gas. Hakansson et al. [25] and Sannes-Lowery and Hofstadler [26] have recently reported on the dissociation for ions trapped in an rf only hexapole trap external to an FTICR mass spectrometer. Pronounced ion dissociation (MSAD) was observed when varying the electrostatic gradient between the skimmer and the hexapole rods (i.e., varying the space charge trapped in the rf only hexapole) [26].

The objective of the present work was to identify experimental parameters for an rf only 2-D quadrupole ion trap that would enable us to control the efficiency of ion fragmentation for extended accumulation periods in an rf only 2-D quadrupole operating as an external trap for an FTICR mass spectrometer. The parameters responsible for the fragmentation onset and selectivity were studied for a variety of molecular ions of different mass-to-charge ratios, charge states, and molecular weights.

Experimental

The 3.5 tesla ESI-FTICR mass spectrometer used in the present studies has been described previously [27–29]. A critical part of the instrument for these studies is the interface for external ion accumulation which consisted of three quadrupoles, all having the same inscribed diameter of 8.2 mm and made of 9.525 mm o.d. stainless steel rods. The middle, 100 mm long quadrupole was used for ion accumulation, operated at a pressure of 5×10^{-4} torr, and was driven by a built-in-house high-Q head controlled by a function generator (model HP 33120A, Hewlett-Packard, Loveland, CO) and an rf amplifier (model 100A150A, Amplifier Research, Souderton, PA). The rods and the 2 mm i.d. input and output conductance limits of the accumulation quadrupole were biased to create the optimal potential well for ion accumulation, cooling, and extraction. The axial potential well in the quadrupole during the accumulation period was defined by the difference between the potentials applied to the conductance limits and quadrupole rods. The radial potential well, $\varphi^*(r)$, was defined as the effective potential, originally introduced by Dehmelt [30] as:

$$\varphi^*(r) = \frac{zeV_{rf}^2}{m\omega_0^2 r_0^2}\left(\frac{r}{r_0}\right)^{2n-2} \quad (1)$$

where V_{rf} is the peak-to-ground rf amplitude, ω_0 is the angular frequency of the rf field, r_0 is the inscribed radius of a quadrupole, m/z is mass-to-charge ratio of an ion, e is the elementary charge, n is the number of pairs of rods of a multipole, and r is the ion coordinate. The ratio between the radial and axial potential wells was adjusted to identify fragmentation patterns of different molecular ions.

The peptide mixtures were dissolved in a water/methanol/acetic acid solution (49:49:2 v%) at concentrations ranged from 0.1 mg/mL to 0.001 mg/mL. All the peptides used in this study (bradykinin, gramicidin S, angiotensin, fibrinopeptide A, γ-endorphin, neurotensin, and melittin) were purchased from Sigma Chemicals (St. Louis, MO) and used without further purification. The solutions were infused into the ESI source at a flow rate of 300 nl/min using a syringe pump (Harvard, South Natick, MA). An Odyssey data station (Finnigan Corp., Madison, WI) was used to control timing and distribution of the potentials, and for data acquisition. Data processing was performed using ICR-2LS software [31].

Results and Discussion

Figures 1a, b, and c show fragmentation patterns for ions generated from a 10^{-5} M mixture of bradykinin, gramicidin S, and angiotensin I (3:3:1 v%) incurred in the rf only accumulation quadrupole. Each spectrum corresponds to a different set of parameters such as ion accumulation time and axial potential well during the accumulation period. One can see that regardless of the accumulation time there is essentially no fragmentation if the axial potential well is below a certain level (2.5 V in Figures 1a, b, and c). However, deepening the axial potential well results in intensive fragmentation (Figures 1d, e, and f), which increases with accumulation time. The mass spectra shown in Figure 1 indicate that under some accumulation quadrupole conditions significantly reduced or suppressed ion fragmentation will occur at longer accumulation times.

It should be mentioned that a small amount of fragmentation (fragment b7,1+ of angiotensin, see Figure 1a) observed at the shortest accumulation time (5 ms) is likely due to the CAD in the quadrupoles upstream of the accumulation quadrupole. The fact that this fragment disappears from the mass spectra at accumulation times >20 ms (see Figures 1b and d) suggests that these species enter the accumulation quadrupole with a significant radial velocity. After gaining additional kinetic energy from the rf field in the accumulation quadrupole, b7,1+ fragments either further decompose in collisions with the background gas to fragments that become unstable in the accumulation quadrupole or oscillate with an amplitude increasing in the fringing rf field, resulting in their instability.

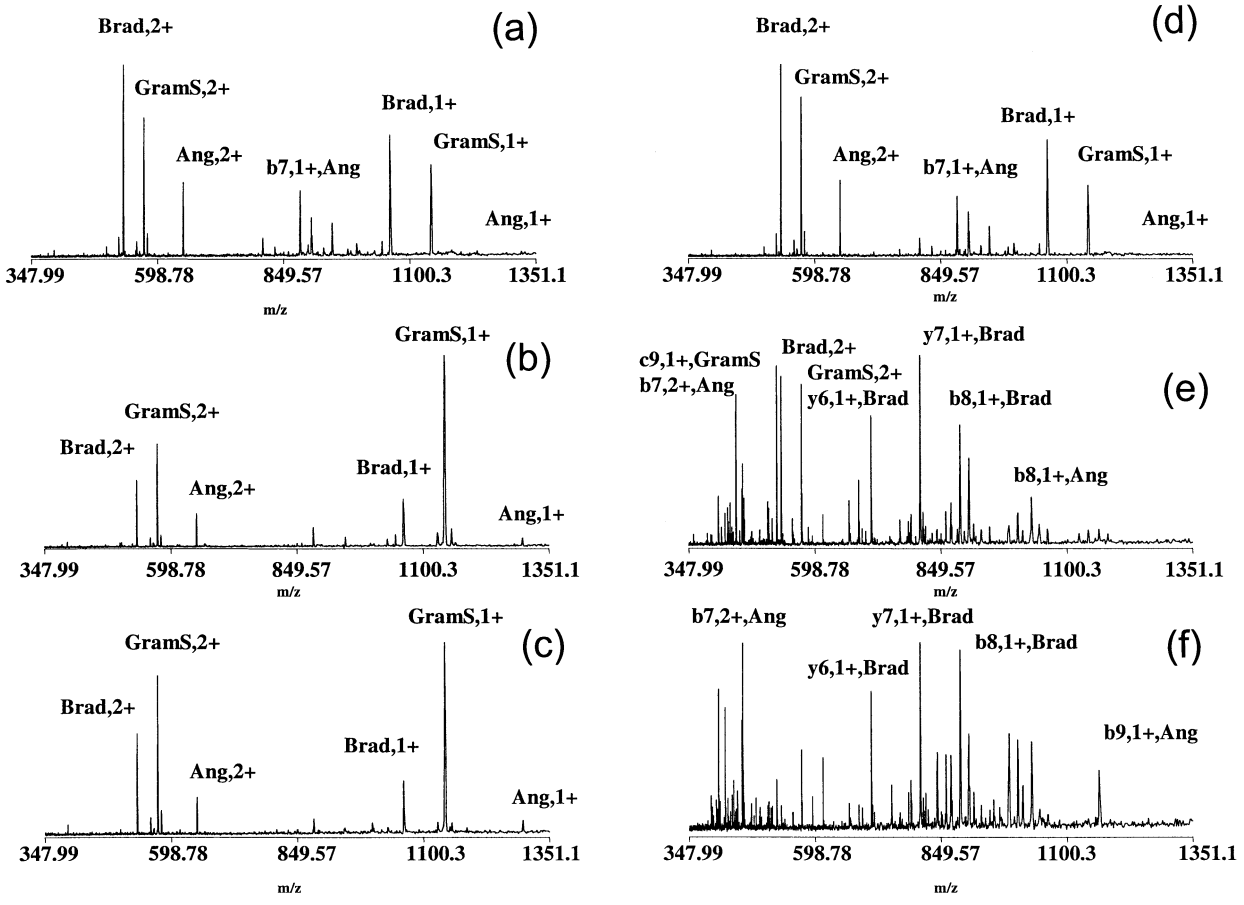

Figure 1. Mass spectra of a 10^{-5} M mixture of bradykinin [Brad], gramicidin S [GramS], and angiotensin I [Ang] (3:3:1 v%) acquired at different axial well depths and accumulation times. Axial well depth was 2.5 V with the accumulation time varying as (**a**) 5 ms, (**b**) 100 ms, and (**c**) 1 s. Axial well depth was 9 V with the accumulation time varying as (**d**) 5 ms, (**e**) 100 ms, and (**f**) 1 s. An rf amplitude was 270 V_{pp} at a frequency of 600 kHz.

In an attempt to reveal the crucial parameters causing ion fragmentation, we studied the fragmentation thresholds (defined here as a 50:50 ratio of intensities for the parent and fragment ions at an accumulation time of 500 ms) for a number of peptides (including bradykinin, gramicidin S, melittin, angiotensin I, neurotensin, fibrinopeptide A, and γ-endorphin) as a function of the radial and axial wells confining an ion cloud inside the accumulation quadrupole.

In Figure 2a we plotted the fragmentation threshold data points for a number of peptides against their *m/z* dependent effective potentials (i.e., radial well depth) and the *m/z* independent electrostatic axial well depth. It was found that all the peptides under study fit the same fragmentation threshold curve within the experimental error independent of their *m/z*. It should be pointed out that since the effective potential is an *m/z* dependent function, the fragmentation threshold data points of different peptides corresponding to the same axial well depth were obtained at different rf amplitudes. To verify that the ratio of the effective potential to the axial well depth is a universal indicator for the onset of ion fragmentation, the rf frequency was varied in the range of 200 kHz (~30% of the high-Q head resonant frequency) keeping the rf amplitude constant. The fragmentation threshold for each peptide (e.g., angiotensin I) was plotted versus the effective potential and the axial well depth in Figure 2b. The thresholds at different rf frequencies match the curve in Figure 2a, obtained with an rf frequency of 600 kHz. A practical conclusion to be drawn from the universality of the fragmentation threshold curve is that by the appropriate choice of quadrupole operation parameters (i.e., rf amplitude and frequency, as well as the bias between the conductance limits and quadrupole rods), both the degree and selectivity of ion fragmentation can be controlled.

Figure 3 shows the mass spectrum of a 10^{-5} M mixture of bradykinin, gramicidin S, and angiotensin I, revealing both singly and doubly charged molecular ions. By changing the dc offset on the accumulation quadrupole rods at a fixed rf field one can control the degree of fragmentation from the intact parent ion mass spectrum (i.e., no fragmentation), to fragmentation of only singly charged ions (doubly charged ions are unaffected), to complete fragmentation of all the parent

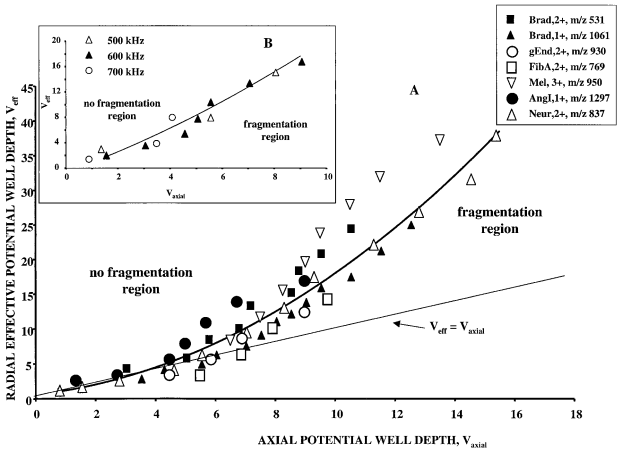

Figure 2. (**a**) Fragmentation thresholds of bradykinin [Brad], γ-endorphyn [γEnd], fibrinopeptide A [FibA], mellitin [Mel], angiotensin I [Ang], neurotensin [Neuro] plotted against the *m/z* dependent radial well depth (i.e., the effective potential in eq. 1) and *m/z* independent axial well depth (i.e., the potential difference between the conductance limit and quadrupole rods). The accumulation time was 500 ms at an rf frequency of 600 kHz. The fragmentation region indicates that at a fixed radial well depth (i.e., fixed rf field) increasing the axial well depth results in the enhanced fragmentation. The no fragmentation region shows that at a fixed axial potential well there are parameters of the rf field (i.e., radial well depths) when no ion fragmentation was observed. (**b**) Fragmentation thresholds of the singly charged ions of angiotensin I [AngI] plotted against the radial and axial well depth at different frequencies. Accumulation time was 500 ms. If superimposed on Figure 1**a**, the fragmentation threshold data points for angiotensin I would match the threshold fragmentation curve obtained for other peptides at a frequency of 600 kHz.

ions present. Interestingly, higher *m/z* singly charged ions were found to be more susceptible to fragmentation with an increase in the axial well depth than their doubly charged counterparts.

Controlled dissociation of parent molecular ions trapped for longer accumulation times (~3.5 s) in an rf only hexapole has been previously reported [26]. This dissociation was controlled by varying the skimmer, or the gate electrode potentials, at a fixed dc bias on the hexapole rods. Higher number of ions in the hexapole reservoir at increased skimmer/gate electrode potentials was assumed to account for parent ion dissociation. Compared to our rf only 2-D quadrupole trap experiments, the hexapole ion trap has a flatter bottom in the effective potential well distribution, governed by $\sim(r/r_0)^4$ (see eq 1 for the quadrupole ion trap). Therefore, the space charge driven ion expansion in the hexapole is more pronounced than that in the quadrupole, and ions energy exchange with rf field followed by dissociation in ion-neutral collisions is more likely as well.

Another mechanism for selected ion decomposition has recently been reported in a molecule ion reactor (MIR) [32]. Ions were fragmented on the fly through a segmented quadrupole operating at a pressure of 3 torr. The observed fragmentation in MIR with increasing rf amplitude was explained that lower *m/z* (higher charge state) ions approach the boundary effect activated dissociation conditions (e.g., [21]) when the rf heating of the ions having higher stability parameter *q* (close or even above 0.91) results in extensive collision induced dissociation (CID). Higher *m/z* ions were collisionally activated in the MIR at higher axial gradients through the quadrupole. In this work the stability parameter, *q*, was in the range from 0.3 to 0.6 and axial gradients between the conductance limit and quadrupole rods (~3–9 V) were far below those employed in MIR (~200 V).

To estimate the effect of the radial component of the electric field between the conductance limits and quadrupole rods on ion cloud radial expansion we modeled ion trapping in an rf only quadrupole using SIMION 7.0 [33]. Packets of singly, doubly and triply charged bradykinin ions were simultaneously injected into a 100 mm long, 4.1 mm field radius rf only quadrupole operating at an rf frequency of 450 kHz and a peak-to-peak amplitude of 180 V. The ion's starting positions were randomly distributed over an area of 1 mm in diameter and the initial angles of ion trajectories were randomized over a solid angle of 45°. Three hundred particles, each mimicking a micro ion with a space charge of 10^{-13} C (i.e., a total space charge of $\sim 10^8$ elementary charges) were employed to model ion–ion interactions. Ion-neutral interactions were modeled using hard-sphere collisions (at a pressure of 5×10^{-5} torr) using a relaxation mean free path for a linear damping term and randomized ion scattering after each collision. The quadrupole rods were biased at 8 V and the exit conductance limit was kept at a potential of 20 V. After passing the acceleration region between the entry conductance limit and quadrupole rods ions acquired nominal axial energies determined by a potential difference between these elements at the start of the simulation. This simulation enabled us to estimate a number of parameters characteristic of rf only quadrupole ion trapping, including relaxation times and lengths for different *m/z* ion species, radial and axial separations of the ion cloud, and of particular interest here, the effect of the radial component of the electric field between the conductance limits and the quadrupole rods on the ion radial expansion at different axial well depths. This effect was studied by examining ion radial distributions at the first turnaround point of ion trajectories. Figures 4a, b, c, and d show the radial distributions for singly and triply charged ions of bradykinin at the first turnaround point near the exit conductance limit for axial potential well depths of 2 and 12 V, corresponding to dc biases on the entry conductance limit of 10 and 20 V, respectively. At an axial well depth of 2 V the ion turnaround point was found to be 6 mm away from the exit conductance limit, inside of the accumulation quadrupole. A 12 V axial well depth was characterized by an ion turnaround point located in close proximity to the exit conductance limit, where ions are more strongly affected by the radial component of the dc field and fringing rf field. Figures 4a, b, c, and d demonstrate that both singly and triply charged ion species have ~2-fold broader ion

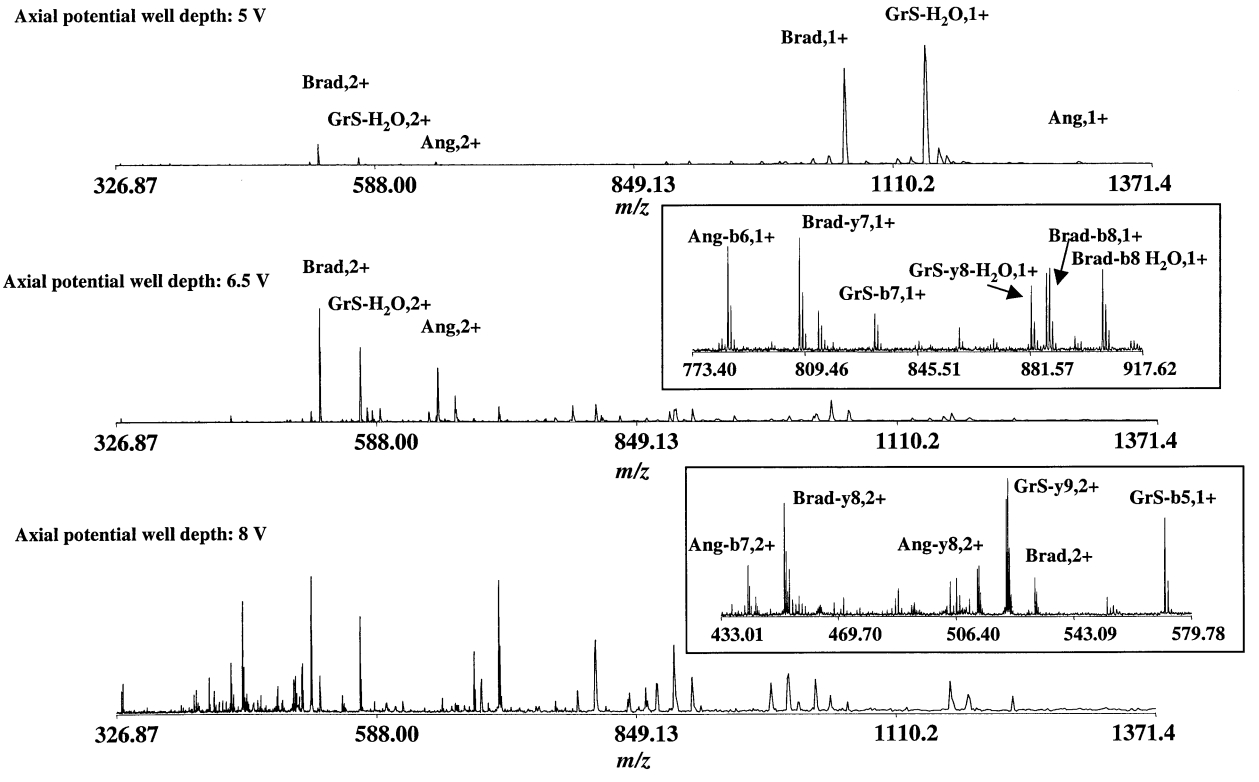

Figure 3. Mass spectra of a 10^{-5} M mixture of bradykinin [Brad], gramicidin S [GramS], and angiotensin I [Ang] (3:3:1 v%) acquired at different axial well depths and an accumulation time of 500 ms. The rf amplitude was 400 V_{pp} at an rf frequency of 600 kHz. Increasing the axial well depth resulted in selective fragmentation of different molecular species, with higher *m/z* ions fragmenting at lower de offsets.

radial distributions at the deeper axial well depth, implying larger rf amplitude oscillations prior to final collisional ion damping. Note that at any fixed axial well depth singly charged ion species have broader radial distribution than their triply charged counterparts.

Based on the simulation results, we believe that the radial component of the electric field between the conductance limits and quadrupole rods along with the space charge repulsion are the major contributors to the radial expansion of the ion cloud in the accumulation quadrupole. Radial ion expansion is governed by the balance between the confining effective potential force, F_{eff}, and the radial component of the dc electric field, F_{dc_rad}, superimposed over the radial component of the space-charge repulsion force, F_{sc_rad}, directed towards the quadrupole rods (the space charge repulsion force directed towards the quadrupole axis is cancelled out due to cylindrical symmetry). Ions entering the quadrupole lose their kinetic energy in collisions with neutrals and come to a complete stop at a turnaround point near the rear conductance limit. Further oscillations in the accumulation quadrupole depend on the aforementioned balance of forces. The balance of forces is, in turn, a function of the mass-to-charge ratio and charge states of ions, because $F_{eff} \sim z^2/m$, and $F_{dc\_rad} + F_{sc\_rad} \sim z$. Therefore, higher *m/z* ions (i.e., less efficiently confined by the effective potential) drift closer to the rods, thus acquiring larger amplitudes of radial oscillations inside the quadrupole and become more prone to fragmentation. This would explain, for example, why singly charged ions fragment at lower axial potential well depths than those required for fragmentation of their doubly charged counterparts (see Figure 3).

It should be noted that even for lower space charge (e.g., relatively short accumulation time of 100 ms in Figure 1b) there is a significant degree of ion fragmentation at deeper axial well depths, supporting the assumption on radial ion expansion due to the radial component of the dc electric field. At a pressure of 5×10^{-4} torr the mean free path of bradykinin ions is about 1 cm, assuming a cross section of 800 A^2. The ion's energy of *z*-oscillations is collisionally damped after ~three passages across the quadrupole (i.e., the relaxation length is about 30 cm), thus resulting in squeezing the ion cloud to the middle of the quadrupole where ions will not be activated by the radial dc field. Without radial expansion the ions would experience ~30 collisions in three passages. With the radial expansion we estimate that prior to being collisionally damped, ~50 collisions with the buffer gas is sufficient for ion fragmentation. Adding more ions to the quadrupole (i.e., increasing the space charge) increases the time for

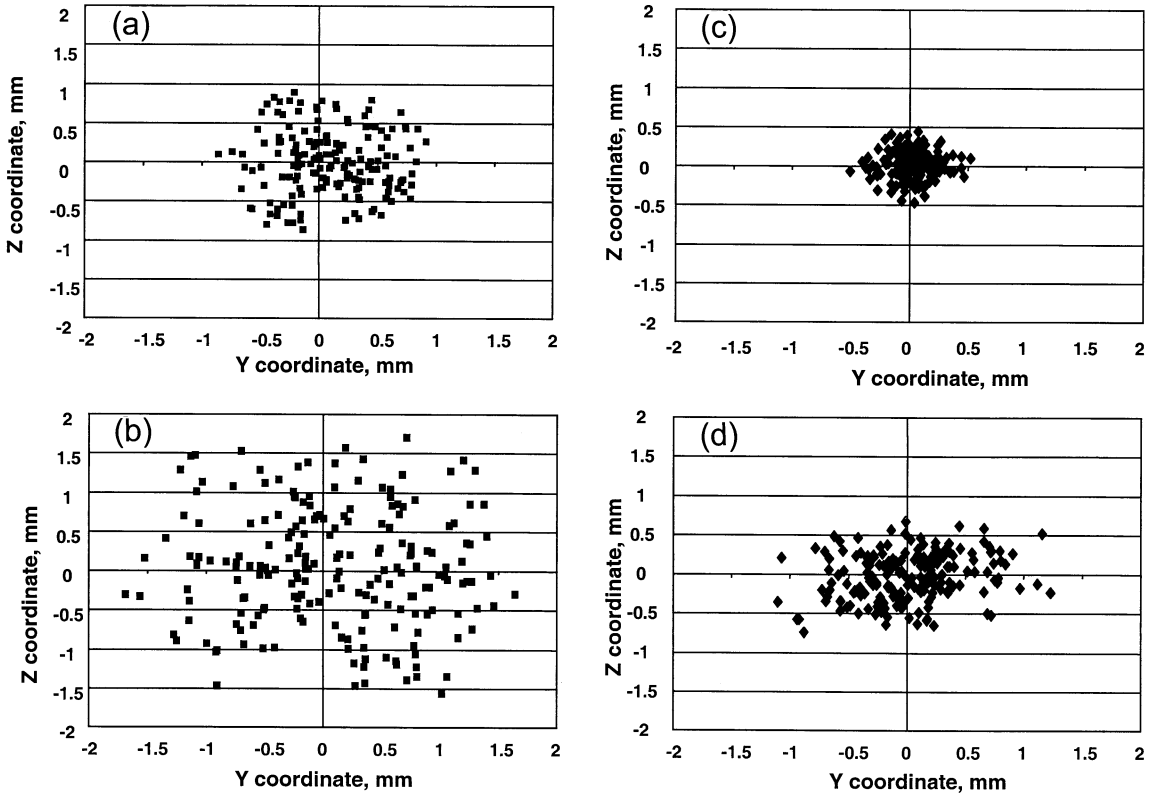

Figure 4. SIMION 7.0 modeled radial distributions of bradykinin ions in the first turnaround point of ion trajectories in the accumulation quadrupole. Each data point represents a micro ion carrying a charge of 10^{-13} C. (**a**) singly charged ions trapped at an axial well depth of 2 V; (**b**) singly charged ions trapped at an axial well depth of 12 V; (**c**) triply charged ions trapped at an axial well depth of 2 V; (**d**) triply charged ions trapped at an axial well depth of 12 V. The X-axis coincides with the quadrupole axis.

energetic ion neutral interactions, since ions are pushed to the region of higher dc and rf field by ion–ion interactions. Further increase in the axial potential well at a fixed rf amplitude and frequency shifts the balance of the radial forces, so that doubly charged ions expand to the radii where they begin to oscillate to amplitudes sufficient to induce fragmentation.

Interestingly, the threshold fragmentation curve deviates from the relationship $V_{\text{eff}} \sim V_{\text{axial}}$ at deeper radial/axial potential wells (see Figure 2). This deviation is believed to be related to a greater contribution from the space charge and larger rf amplitudes due to a reduction in the maximum q Mathieu for which the ions will be stable. We have recently reported [34] that with increasing the space charge trapped in the accumulation quadrupole, the ion stability diagram distorts, reducing q_{max} to about 0.7. The highest q observed for doubly charged bradykinin was about 0.65, thus making boundary effect activated dissociation very effective at a small increase in the axial field gradient. The upper boundary of the nonfragmentation region shown in Figure 2 is, then, defined by the ion stability parameter, q.

It should be noted that increasing pressure in the accumulation quadrupole would result in better collisional focusing and decrease in the radial component of ion velocity. However, the number of collisions would increase proportionally to the increase in the pressure. If the kinetic energy gained by an ion on its mean free path exceeds the dissociation threshold, ion fragmentation would still be a factor. Therefore, to suppress ion fragmentation, the pressure in the accumulation quadrupole should be raised significantly ($\sim 10^{-2}$ torr). This elevated pressure would extend ion ejection from the quadrupole, resulting in lower efficiency of gated trapping in the FTICR cell.

To summarize, fragmentation of ions trapped in 2-D accumulation quadrupole can be controlled by adjusting the ratio of the potential difference between the trapping plates (i.e., conductance limits) and quadrupole rods and the effective potential of the rf field. At shorter accumulation times (lower space charge), if the trapping voltage is too high, the radial component of the increased dc field deflects ions to larger radii, where they exhibit larger amplitude oscillations because of higher rf field and decompose in collisions with the buffer gas. At longer accumulation times (higher space charge) both the dc field and space charge repulsion increase the ion cloud radius, thus causing increased fragmentation. In order to avoid fragmentation at a

fixed axial well depth and for any extended accumulation period, the radial well depth (i.e., the effective potential) needs to be increased, so that ions are confined to smaller radii and cannot gain kinetic energy from the rf field sufficient for their collision induced fragmentation. The increase in the effective potential (stronger radial confinement) is limited by ion instability ($q \sim \varphi^*_{\text{eff}}/V_{\text{rf}}$). At deeper axial well depths higher space charge narrows the ion stability diagram ($q_{\max} \sim 0.7$ [34]) imposing constrains for further increasing the effective potential (i.e., increasing the effective potential accompanied by the increase in q up to 0.7 causes boundary effect activated dissociation).

In the present work we provide a simplified explanation for ion fragmentation in an rf only accumulation quadrupole, and additional theoretical insights are required to quantitatively understand the observed phenomena. We have focused on the fragmentation of model peptides similar in molecular weights and structures to the tryptic peptides detected in the course of LC separations of cellular protein digests. However, it has yet to be explained why higher molecular weight ions (e.g., melittin) fit the same threshold fragmentation curve in Figure 2a. We would expect the threshold fragmentation curve to be more molecular weight dependent, since large molecules can require more internal energy before dissociation occurs and thus, are expected to be characterized by the increased dissociation thresholds. The investigation of dissociation thresholds for heavier molecules trapped in the accumulation quadrupole (e.g., proteins) requires further generalization of the fragmentation mechanisms.

Conclusions

In this work we have demonstrated that there is a set of experimental conditions under which we can control the fragmentation of ions trapped in a 2-D rf only quadrupole. We have found that the onset, selectivity, and degree of ion fragmentation are functions of the ratio of the effective potential (radial well depth) to the axial trapping potential (axial well depth). Depending on the ratio of the axial/radial well depths, ions of different mass-to-charge ratios can be detected as either intact or dissociated species. Interestingly, the ratio of the axial/radial well depths appears to be a universal indicator for the fragmentation threshold independent of the ion's mass-to-charge ratio, charge state and molecular weight. For extended accumulation periods (seconds) and deeper axial well depths, implying higher space charge in the accumulation quadrupole, we identified the parameters of the rf field where no fragmentation was observed. An ion fragmentation mechanism, based on ion radial expansion due to the radial components of the dc field and space charge followed by larger amplitude oscillations in higher rf field and collision induced dissociation, has been proposed. The capability of controlling the fragmentation of peptide ions trapped in the accumulation quadrupole external to an FTICR mass spectrometer is very important in proteomic studies and can potentially be used to reveal structural information on the detected molecular species (e.g., in the course of LC separation the parent ion mass spectrum would be followed by the spectrum of fragmentions).

Acknowledgments

This research was supported by the NIH National Center for Research Resources (RR12365), and the Office of Biological and Environmental Research, U.S. Department of Energy. MVG thanks Russian Basic Sciences Foundation for the support of his research activities under grant 99-04-49261, as well as Associated Western Universities Inc. (AWU). Pacific Northwest National Laboratory (PNNL) is a multiprogram national laboratory operated by Battelle Memorial institute for the U.S. Department of Energy under Contract DE-AC06-76RLO 1830.

References

1. Jensen, P. K.; Pasa-Tolic, L.; Anderson, G. A.; Horner, J. A.; Lipton, M. S.; Bruce, J. E.; Smith, R. D. *Anal. Chem.* **1999,** *71,* 2076–2084.
2. Veenstra, T. D.; Martinovich, S.; Anderson, G. A.; Pasa-Tolic, L.; Smith, R. D. *J. Am. Soc. Mass Spectrom.* **2000,** *11,* 78–82.
3. Shen, Y.; Zao, R.; Belov, M. E.; Conrads, T. P.; Anderson, G. A.; Tang, K.; Pasa-Tolic, L.; Veenstra, T. D.; Lipton, M. S.; Smith, R. D. *Anal. Chem.* **2001,** *73,* 1766–1775.
4. Senko, M. W.; Hendrikson, C. L.; Emmett, M. R.; Shi, S. D.-H.; Marshall, A. G. *J. Am. Soc. Mass Spectrom.* **1997,** *8,* 970–976.
5. Wang, Y.; Shi, S. D.-H.; Hendrickson, C. L.; Marshall, A. G. *Int. J. Mass Spectrom.* **2000,** *198,* 113–120.
6. Belov, M. E.; Nikolaev, E. N.; Anderson, G. A.; Udseth, H. R.; Conrads, T. P.; Veenstra, T. D.; Masselon, C. D.; Gorshkov, M. V.; Smith, R. D. *Anal. Chem.* **2001,** *73,* 253–261.
7. Belov, M. E.; Nikolaev, E. N.; Anderson, G. A.; Auberry, K. J.; Harkewicz, R. Smith R. D. *J. Am. Soc. Mass Spectrom.* **2001,** *12,* 38–48.
8. Sannes-Lowery, K.; Griffey, R. H.; Kruppa, G. H.; Speir, J. P.; Hofstadler, S. A. *Rapid Commun. Mass Spectrom.* **1998,** *12,* 1957–1961.
9. Smith, R. D. *Int. J. Mass Spectrom.* **2000,** *200,* 509–544.
10. Shen, Y.; Tolic, N.; Zao, R.; Pasa-Tolic, L.; Li, L.; Berger, S. J.; Harkewicz, R.; Anderson, G. A.; Belov, M. E.; Smith, R. D. *Anal. Chem.* **2001,** *73,* 3011–3021.
11. Yost, R. A.; Enke, C. G.; McGilvery, D. C.; Smith, D.; Morrison, J. D. *Int. J. Mass Spectrom. Ion Processes* **1979,** *30,* 127.
12. Shushan, B.; Douglas, D. J.; Davison, W. R.; Nacson, S. *Int. J. Mass Spectrom. Ion Processes* **1983,** *46,* 71–74.
13. Dawson, P. H.; Fulford, J. E. *Int. J. Mass Spectrom. Ion Processes* **1982,** *42,* 195–211.
14. Boyd, R. K. *Mass Spectrom. Rev.* **1994,** *13,* 359–410.
15. Mansoori, B. A.; Dyer, E. W.; Lock, C. M.; Bateman, K.; Boyd, R. *J. Am. Soc. Mass Spectrom.* **1998,** *9,* 775–788.
16. Douglas, D. J.; French, J. B. *J. Am. Soc. Mass Spectrom.* **1992,** *3,* 398–408.
17. March, R. E.; Hughes, R. J. *Quadrupole Storage Mass Spectrometry.* Wiley: Toronto, 1989, p 365–378.
18. March, R. E.; Todd, J. F. J. *Practical Aspects of Ion Trap Mass Spectrometry, Vol. I.* CRC Press: Boca Raton, 1995, p 303–341.
19. Dawson, P. H. *Quadrupole Mass Spectrometry and Its Applications.* Elsevier Scientific: New York, 1976, p 195–201.
20. Creaser, C. S.; O'Neil, K. E. *Org. Mass Spectrom.* **1993,** *28,* 564–569.
21. Paradisi, C.; Todd, J. F. J.; Traldi, P.; Vettori, U. *Org. Mass*

Spectrom. **1992,** *27,* 251–254.
22. Fischer, E. *Z. Phys.* **1959,** *156,* 26.
23. Sheretov, E. P.; Zenkin, V. A.; Samorodov, V. F. *Sov. Phys. Tech. Phys.* **1973,** *18,* 282–283.
24. Todd, J. F. J.; Waldren, R. M.; Mather, R. E. *Int. J. Mass Spectrom.* **1980,** *34,* 325–349.
25. Hakansson, K.; Axelsson, J.; Palmblad, M.; Hakansson, P. *J. Am. Soc. Mass Spectrom.* **2000,** *11,* 210–217.
26. Sannes-Lowery, K. A.; Hofstadler, S. A. *J. Am. Soc. Mass Spectrom.* **2000,** *11,* 1–9.
27. Belov, M. E.; Gorshkov, M. V.; Udseth, H. R.; Anderson, G. A.; Tolmachev, A. V.; Prior, D. C.; Harkewicz, R.; Smith, R. D. *J. Am. Soc. Mass Spectrom.* **2000,** *11,* 19–23.
28. Belov, M. E.; Gorshkov, M. V.; Anderson, G. A.; Udseth, H. R.; Smith, R. D. *Anal. Chem.* **2000,** *72,* 2271–2279.
29. Gorshkov, M. V.; Pasa-Tolic, L.; Udseth, H. R.; Anderson, G. A.; Huang, B. M.; Bruce, J. E.; Prior, D. C.; Hofstadler, S. A.; Tang, L.; Chen, L. Z.; Willett, J. A.; Rockwood, A. L.; Sherman, M. S.; Smith, R. D. *J. Am. Soc. Mass Spectrom.* **1998,** *9,* 692–700.
30. Dehmelt, H. G. *Adv. Atom. Mol. Phys.* **1967,** *3,* 53–72.
31. Anderson, G. A.; Bruce, J. E. *ICR-2LS Software Package*, PNNL.
32. Dodonov, A.; Kozlovsky, V.; Loboda, A.; Raznikov, V.; Sulimenkov, I.; Tolmachev, A.; Kraft, A.; Wollnik, H. *Rapid Commun. Mass Spectrom.* **1997,** *11,* 1649–1656.
33. DahlD. H. *SIMION 3-D, Version 7.0*, User's Manual, 2000.
34. Belov, M. E.; Nikolaev, E. N.; Harkewicz, R.; Masselon, C. D.; Alving, K.; Smith, R. D. *Int. J. Mass Spectrom.* **2001,** *208,* 205–225.